CRACK SHIELDING MECHANISMS OF INTERLAYERED EPOXY MATERIALS UNDER QUASI-STATIC AND FATIGUE LOADING

Dharun Vadugappatty Srinivasan and Anastasios P. Vassilopoulos

[1] Composite Construction Laboratory (CCLab), Ecole Polytechnique Fédérale de Lausanne (EPFL), Station 16, CH-1015 Lausanne, Switzerland.

Keywords: Fracture, Fatigue, Epoxy, Thermoplastics, Composites, Configurational material forces, Crack shielding

ABSTRACT

This research explores the capability of PEI and PVDF thermoplastic interlayers to arrest cracks in epoxy materials modified with short-glass fibers and core-shell rubber particles. It also investigates the effect of interlayer position, the number of interlayers, and the type of epoxy materials on the fracture performance under mode-I quasi-static fracture and fatigue loading in a single-edge-notch bending configuration. The quasi-static fracture results demonstrate that the thermoplastic-epoxy interface effectively arrests the initial crack and reinitiating the crack at the thermoplastic layer requires up to 2.5 times higher load than the crack initiation load of the pristine epoxies. Furthermore, the interlayered designs exhibit up to 43 times more energy absorption than their pristine counterparts, and the study captures the competing damage mechanisms and failure events using microscopic images, digital image correlation, and high-speed photography observations.

1 INTRODUCTION

High-performance polymeric materials are commonly used in lightweight structures, where specific strength, stiffness, and damage tolerance requirements must be met. However, achieving high strength and toughness together is challenging, although many natural materials, typically multi-scale composites, exhibit various toughening mechanisms under damage and therefore, possess both qualities. Material inhomogeneity, which is achieved by combining two or more materials to form distinct interfaces, is considered the “universal” strategy for enhancing fracture toughness. Different materials can be combined based on their tensile modulus, yield strength, and hardening coefficient/plasticity and they are classified as E-inhomogeneity, σ_y inhomogeneity, and n-inhomogeneity, respectively [1]. Different cases, including hard to soft transition, soft to hard transition, and weak hardening coefficient to strong hardening coefficient, have implications on crack-tip shielding or anti-shielding [2–5]. To achieve a good crack-arresting interlayered design, a large difference between the pristine and interlayer material properties is recommended. Although increasing interlayer thickness can enhance fracture toughness, this does not apply to all scenarios [6]. Toughened epoxy materials are commonly used to increase damage-tolerance in engineering applications, such as in wind turbines and aerospace adhesive joints. Hybrid adhesives have been developed to improve static and fatigue properties [7,8]. To control the crack path, interlayer epoxy adhesive bond lines can be designed. Additionally, finite element models have been developed to simulate crack-tip phenomena using small-scale yielding theory, J integrals, and configurational material forces theory.

Using compliant interlayer materials have several disadvantages, including reduced stiffness, crack-tip anti-shielding, and questionable structural integrity of the compliant interlayers for high-temperature applications. It is also unclear whether highly toughened thermoplastics can be used as interlayer materials, regardless of their modulus and strength. Investigating alternative combinations is necessary to explore this hypothesis, as there is currently no research on the far and unstable crack-arresting capability of thermoplastic interlayers in epoxy materials.

This study uses polyvinylidene fluoride (PVDF) and polyetherimide (PEI) thermoplastic layers of 0.5 mm thickness modified with short-glass fiber and core-shell rubber toughened epoxy materials. Uniaxial tensile experiments are used to determine the constitutive properties of all materials, and the damage tolerance is examined through single-edge-notch bending (SENB) specimens under 3-point

bending mode-I quasi-static fracture loading. The study investigates the effect of interlayer position, the number of interlayers, and hybrid epoxy materials on fracture behavior. The failure mechanisms are documented using microscopic images, digital image correlation, and high-speed photographs. In an on-going study, the selected designs are subjected to mode-I fatigue loading to determine the fatigue crack growth-arresting capability of the interlayered materials.

2 MATERIALS AND MANUFACTURING

SPABOND™ 820HTA and SPABOND™ 840HTA epoxy materials were provided by Gurit (UK) Ltd provided and were used to make pristine and interlayered SENB specimens. SP 820HTA contains short-glass fibers and is non-toughened, while SP 840HTA contains core-shell rubber particles and is toughened. Amorphous thermoplastic materials, Natural Kynar® PVDF and Ultem® 1000 PEI were procured from Emco Industrial Plastics, Inc, USA for interlayering and uniaxial tensile experiments.

To conduct the tensile experiments, 4 mm-thick panels of both non-toughened (BB) and toughened (TT) epoxy materials were produced through the following steps. The epoxy base and hardener materials were manually blended in a weight ratio of 100:34 using a wooden spatula, then degassed at 0.95 bar of vacuum for 7 minutes. Afterward, the mixture was applied into an aluminum mold, coated with a release agent (Sika® liquid wax- 815), and left to cure at 20 ± 2°C for 2 hours. The panels were then cured inside a convection oven at 70°C for another 2 hours, with a heating and cooling rate of 2 ^{o}C/min and 5 ^{o}C/min, respectively. The cured panels were cut into ASTM D638-22 Type I specimens. As for the PEI and PVDF thermoplastics, Type I specimens were cut from the 3 mm-thick plates purchased as is.

Specimen	Epoxy	IL material	IL nominal position (mm)
BB	BB	-	-
BBA1U	BB	PEI	1.5
BBA1K	BB	PVDF	1.5
BBA2U	BB	PEI	6.75
BBA2K	BB	PVDF	6.75
BTA1U	BB & TT	PEI	1.5
TT	TT	-	-
TTA1U	TT	PEI	1.5
TTA1K	TT	PVDF	1.5
TTA2U	TT	PEI	6.75
TTA2K	TT	PVDF	6.75
TTA1KK	TT	PVDF	1.5, 3

Table 1: SENB specimen designs for quasi-static fracture experiments.

The fracture experiments were conducted using SENB (Single Edge Notched Bend) specimens with dimensions of 132 mm × 30 mm × 15 mm. Pristine and interlayered epoxy SENB specimens were obtained from blocks of epoxy material, which were fabricated using aluminum molds and the same epoxy mixing and curing process as described previously. To investigate the crack-arresting ability of thermoplastic layers in near and far-crack scenarios, two molds were utilized to allow the placement of the thermoplastic layers at two distinct positions (A1= 1.5 mm and A2= 6.75 mm) from the initial notch tip. Additionally, two special designs were studied: (i) the BTA1U specimen, which is a hybrid epoxy material consisting of BB and TT epoxy material separated by a PEI interlayer that can be mixed and cured concurrently, and (ii) the TTA1KK specimen, which is a dual-interlayered specimen that has two PVDF layers with an inter-distance of approximately 1.5 mm. Table 1 shows the different specimen configurations used for fracture experiments.

3 EXPERIMENTAL AND NUMERICAL METHODS

3.1 Uniaxial tensile experiments

An MTS® 810 Landmark servo-hydraulic machine, equipped with a 5 kN load cell and ±0.2% load accuracy was used for conducting uniaxial tensile experiments of epoxy and thermoplastic materials. ASTM D638-22 Type I tensile specimens were tested under displacement control at a rate of 1 mm/min, while 2D digital image correlation (DIC) measured the engineering strain field on the specimens' surface.

3.2 Fracture experiments

A Walter+Bai (w+b) electromechanical machine, with a load cell capacity of 50 kN and applied compression load accuracy of 0.09% was used for conducting quasi-static fracture experiments at an ambient temperature of 22 ± 3°C and relative humidity of 40 ± 10%. ASTM D5045-14 recommended specimen geometry, span-width ratio, initial notch-width ratio, roller diameter, and loading rate (1 mm/min) were maintained. The three-point bending fixture, consisting of three steel rollers (left, right, and top) with a diameter of 20 mm, supported the left and right rollers fixed at a 120 mm span. The initial notch and the contact point of the top roller were on the same loading axis, and DIC images (2D) captured the specimen surface strain field at a 0.5 Hz frequency during the experiments. FASTCAM SA-Z camera Photron® with AF-S NIKKOR 50 mm lens captured high-speed photographs at an imaging frequency of 60,000 frames per second to record failure events. Two to four specimens were tested per design, depending on the experimental scatter.

An MTS® Acumen electromechanical machine equipped with a 3 kN load cell and a three-point bending fixture was used for applying load-controlled sinusoidal patterns at a load ratio of 0.5. To initiate the fatigue loading, all specimens were loaded under displacement control at a rate of 1 mm/min to attain the prescribed mean cyclic load level. After reaching this point, sinusoidal cyclic loads up to the maximum cyclic load (0.5 times the quasi-static fracture load) were applied under load control at 5 Hz, until failure. DIC images and normal photographs were captured at the maximum load of each cycle to calculate the crack growth length. The same ambient conditions were maintained for the fatigue experiments.

4 RESULTS AND DISCUSSION

4.1 Uniaxial tensile behavior

Fig. 1a and 1b show the strength versus modulus and tensile toughness versus true tensile failure strain plots of materials, indicating that selecting different epoxy-thermoplastic combinations can achieve E-inhomogeneity, σ-inhomogeneity, and their combinations. For example, the combination of BB-PEI and TT-PVDF materials creates a hard to soft transition for E-inhomogeneity, but a soft to hard transition for σ-inhomogeneity and G-inhomogeneity. The selected thermoplastic layers possess high fracture energy and can be either compliant or stiffer than epoxy. Finite element modeling was used to evaluate the impact of these mismatches in modulus, strength, and toughness on the crack driving forces.

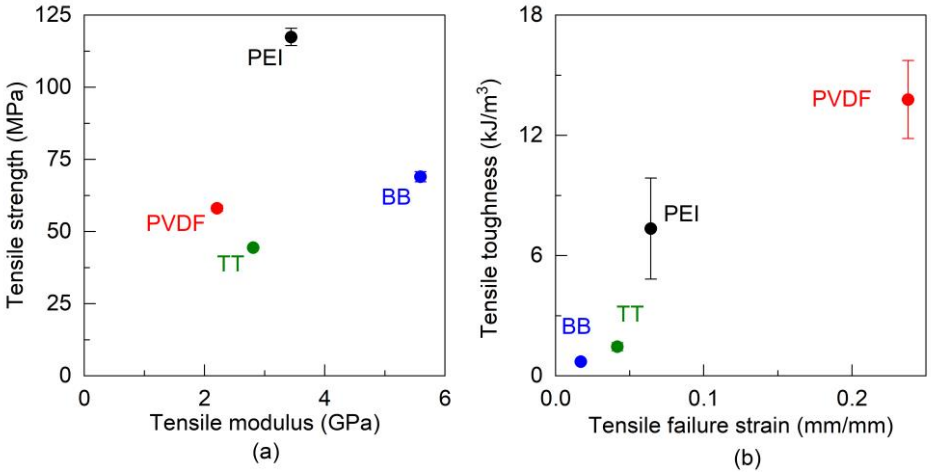

Figure 1: Comparison of the tensile properties (a) modulus versus strength and (b) true tensile failure strain versus tensile toughness.

3.4 Fracture behavior

Fig. 2 presents a comparison of the load and displacement response of the epoxy specimens modified with near-positioned PEI and PVDF interlayering, and non-toughened BB epoxy specimens. All specimens showed a non-linear region initially, but BB epoxy material displayed a linear increase in load up to a maximum of 829 N. PEI and PVDF interlayered specimens exhibited linear increases in load, and the initial peak load was 778 N and 605 N, respectively (stage 1, Fig 2 and Fig 3). In BB-PEI specimens, a cohesive crack and interface crack was formed, and the interface crack was arrested by the PEI layer, a typical Cook–Gordan model of the crack-stopping mechanism. Further increase in displacement led to high bending-tensile stresses and debonding of the BB-PEI and BB-PVDF interface before the final catastrophic failure.

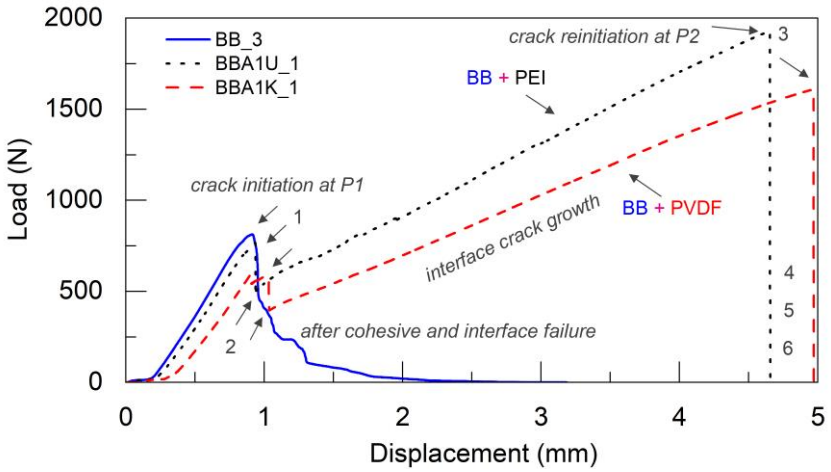

Figure 2: Load versus displacement response: (a) BB_3 epoxy and the near-positioned IL, BB-based SENB specimens (BBA1U_1 & BBA1K_1) and (b) different failure modes of BB-PEI interlayered specimens.

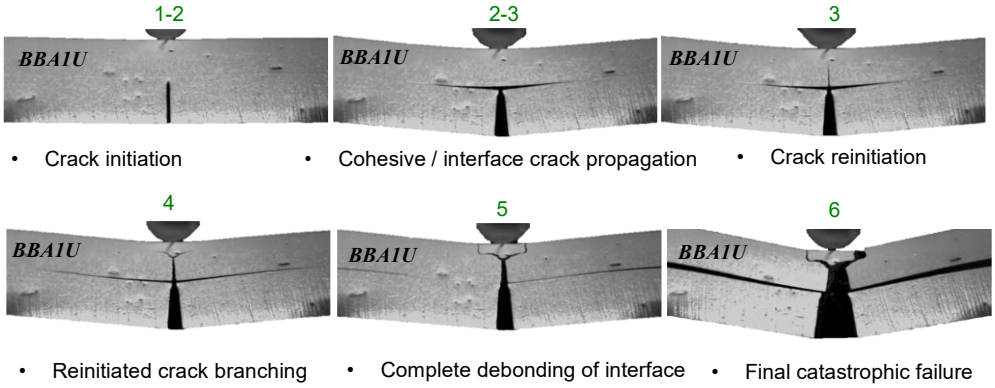

Figure 3: High-speed photographs of the PEI interlayered (BBA1U) specimen during failure.

Fig. 4 presents a comparison of load and displacement responses of pristine (BB) and interlayered epoxy materials with far-positioned PEI (BBA2U) and PVDF (BBA2K). The load-displacement curve of BBA2U shows a linear increase in load until the initial peak load (P1) of 820 N, followed by the initiation of a cohesive crack from the initial notch. The cohesive crack branched into a 'T' shape upon reaching the interface, resulting in a sudden drop in load (stage 2). The crack was shielded by the interface in the near-positioned IL epoxy specimens. After certain interface crack growth, crack reinitiation occurred at the PEI layer (stage 3) at the maximum load (P2) of 744 N, before the final catastrophic failure (stages 4 and 5). The BBA2K interlayered material showed similar failure mechanisms to BBA2U, with initial (P1) and final peak loads (P2) of 758 N and 775 N, respectively. The crack reinitiation load of far-positioned IL specimens was significantly lower than that of near-positioned IL specimens due to an increased crack propagation length of 5.25 mm.

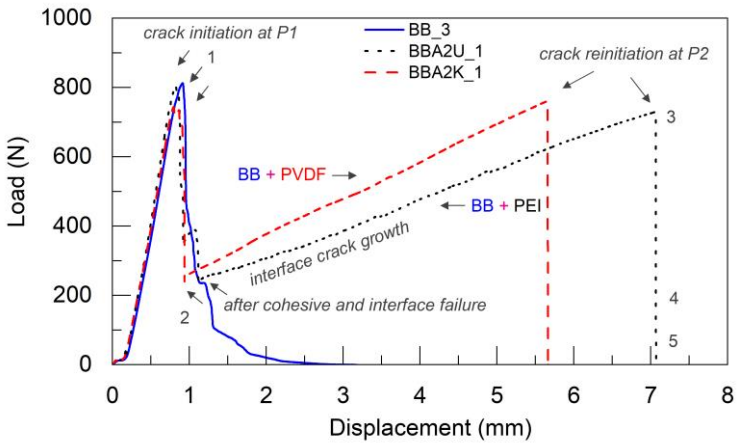

Figure 4: Load versus displacement response of BB_3 epoxy and the far-positioned IL, BB-based SENB specimens (BBA2U_1 and BBA2K_1).

Fig. 5 compares the load and displacement response of three different epoxy specimens: core-shell rubber particle toughened (TT) and interlayered with near-positioned PEI (TTA1U) and PVDF (TTA1K). The TT epoxy material showed a linear increase in load as displacement increased, reaching a peak value of 570 N before a cohesive crack caused a sharp decrease in load resistance. The failure was brittle, but the fracture surface showed a ductile-to-brittle transition region. In the TTA1U interlayered specimens, a sudden drop in load was observed after reaching an initial peak load of 492 N, due to the TT-PEI interface failure. The crack propagated along the interface in a stick-slip nature, leading to high and relatively uniform tensile strain over a region. The plastic energy dissipation resulted

in a highly non-linear load-deflection response before the final fracture at 1540 N. The average crack reinitiation load of PEI interlayered specimens was 2.54 times higher than that of pristine TT epoxy material. The TTA1K interlayered specimens also showed initial non-linear behavior and a slight drop in load resistance due to TT-PVDF interface failure. However, the ligament between the initial notch and interface withstood more load before failing at 383 N. The interface crack was propagated to a certain length after which the TT epoxy material underwent severe plastic deformation, leading to non-linear behavior before the final fracture at 1341 N. Overall, all interlayered specimens exhibited a higher crack reinitiation load than the crack initiation load of pristine TT epoxy material.

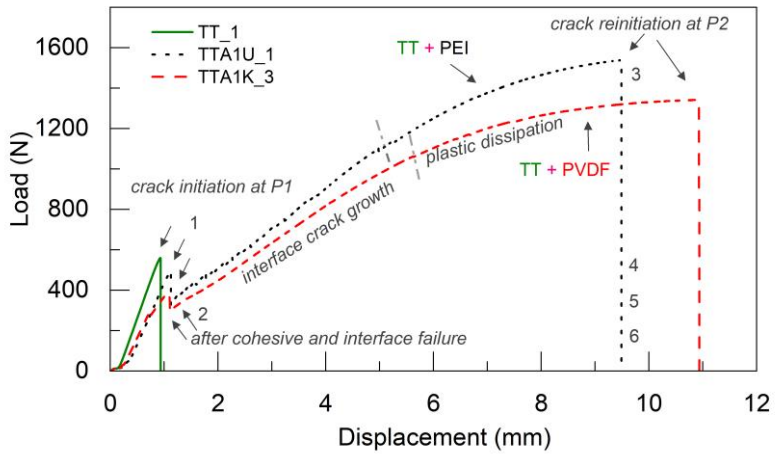

Figure 5: Load versus displacement response of TT_1 epoxy and the near-positioned IL, TT-based SENB specimens (TTA1U_1 & TTA1K_3).

In Fig. 6, the load-displacement response of the pristine (TT) and far-positioned interlayered epoxy materials (TTA2U and TTA2K) is presented. After the initial linear increase, the peak load for TTA2U and TTA2K was 466 N and 469 N, respectively. A cohesive crack was initiated at the notch and propagated in the TT epoxy before deviating due to toughening particles. The crack then propagated along the interface in a stick-slip manner. Unlike near-positioned interlayered materials, TTA2U and TTA2K exhibited a plateau-like behavior before the final failure, which occurred at a higher displacement (~750 N) or ~1.6 times higher than their initial peak load (P1).

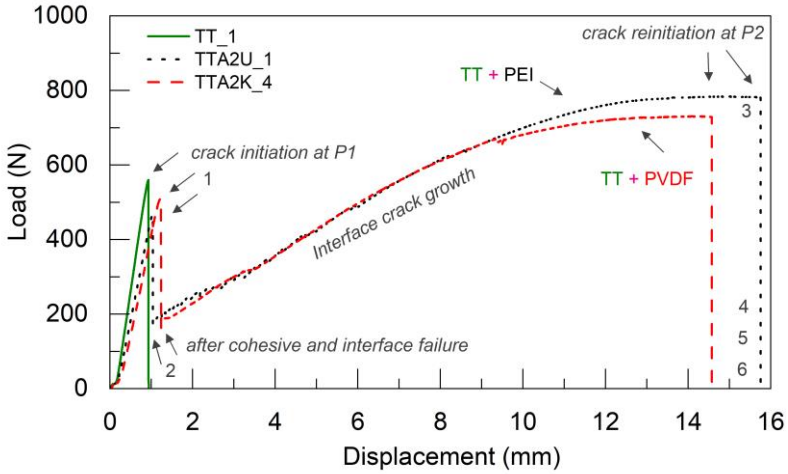

Figure 6: Load versus displacement response of TT_1 epoxy and the far-positioned IL, TT-based SENB specimens (TTA2U_1 and TTA2K_4).

Fig. 7 compares the load-displacement responses of hybrid material designs (BTA1U) and dual interlayering (TTA1KK) with pristine epoxy materials (BB and TT). In BTA1U, the crack initiation load, P1, was comparable to TT epoxy, but the final fracture load, P2, was increased by 180% due to the presence of the PEI layer. In TTA1KK, a non-linear initial slope was observed due to the weak TT-PVDF interface, and the crack propagated along the interface, causing whitened plastic-zone formation between two PVDF interlayers. The crack advanced within the TT epoxy material after the first PVDF interlayer failure and ruptured the second PVDF layer and the remaining TT epoxy.

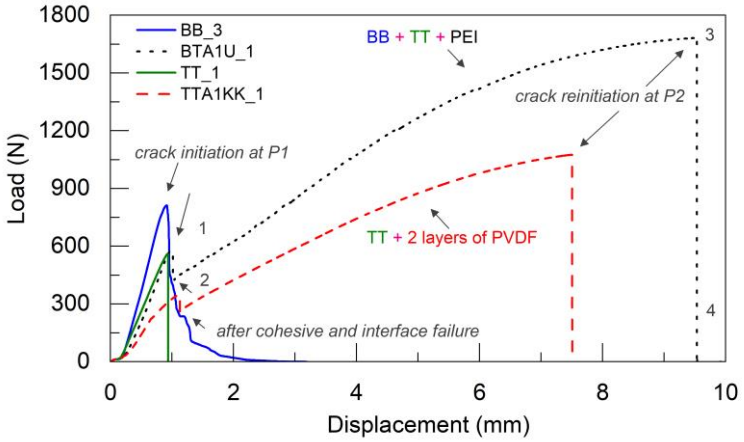

Figure 7: Load versus displacement response of the pristine epoxies (BB_3 & TT_1), hybrid epoxy (BTA1U_1) and dual PVDF interlayered specimens (TTA1KK_1).

The fracture performance of pristine epoxy and interlayered designs was compared in Fig. 8. Initial fracture toughness, load ratio, and normalized area under the load-displacement response were used for the assessment. PEI interlayered epoxy showed no effect on initial fracture toughness, while PVDF interlayered epoxy had a lower initial toughness due to weak interface energy. A slight reduction in initial toughness was observed in other models, but all interlayered designs exhibited crack-shielding behavior beyond the interlayer. The presence of toughened epoxy material in hybrid-material specimens improved energy absorption up to 20 times through PEI interlayer and plastic energy dissipation.

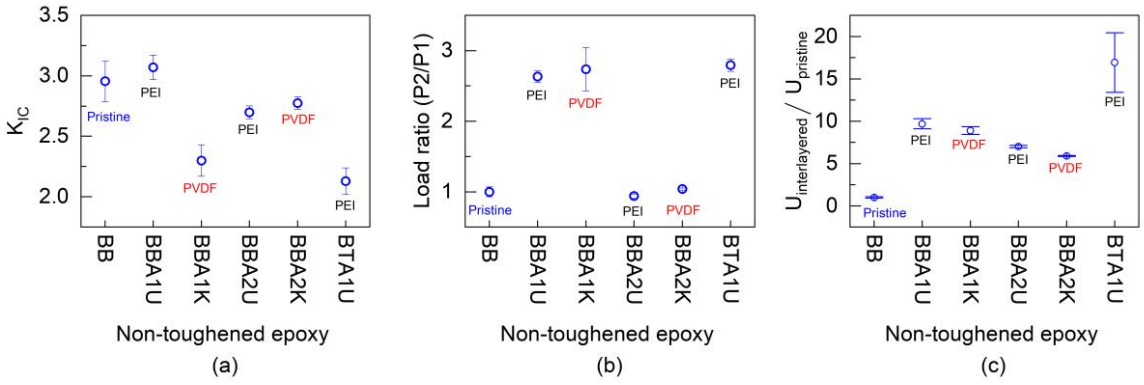

Figure 8: Comparison of fracture characteristics of the non-toughened epoxy-based designs: (a) initial fracture toughness, (b) crack reinitiation to initiation load ratio and (c) energy normalized to the pristine material, BB.

Fig. 9a, 9b, and 9c compare the initial fracture toughness, load ratio (P2/P1), and the normalized area ($U_{interlayered}/U_{pristine}$) under the load-displacement response of the TT-based designs. The presence

of the PEI layer did not affect the initial fracture toughness of the TTA1U material, and no crack-tip shielding or anti-shielding was observed. The high tensile modulus and strength of PEI relative to TT epoxy caused a soft to hard transition that prevented any increase in the crack-driving force. On the other hand, the initial fracture toughness of TTA1K was reduced by 32.4% compared to TT material due to poor compatibility between the epoxy and PVDF interlayer. TTA2U and TTA2K also showed a slight reduction in the initial fracture toughness, despite having higher crack lengths. However, the crack reinitiation load (P2) of these materials was 1.5 times higher than their initial failure load (P1), indicating that the incorporation of thermoplastic layers with toughened material can better enhance damage tolerance through plastic dissipation than with brittle, non-toughened materials. TTA1KK, which had dual PVDF layers in the toughened epoxy material, exhibited crack-driving force enhancement similar to TTA1K. However, it absorbed a relatively 43.5% lower energy due to the formation of a constrained plastic zone.

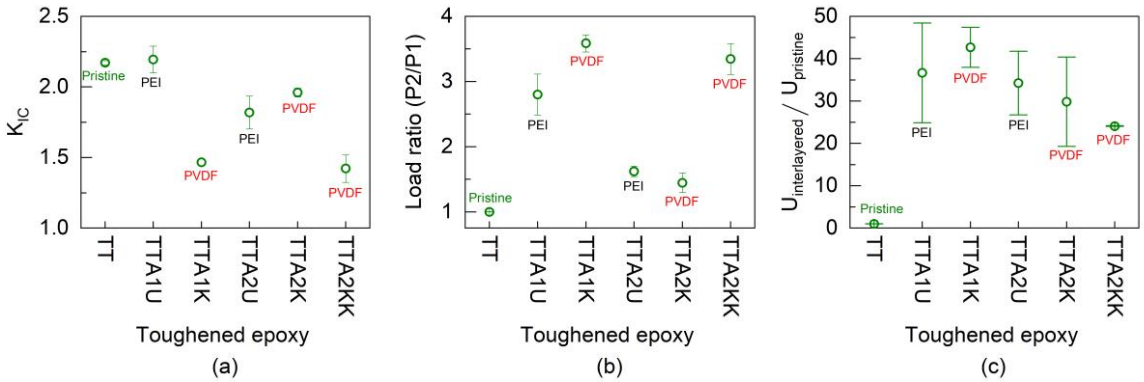

Figure 9: Comparison of fracture characteristics of the toughened epoxy-based designs: (a) initial fracture toughness, (b) crack reinitiation to initiation load ratio and (c) energy normalized to the pristine material, TT.

4 CONCLUSIONS

This study investigated the fracture performance of short-glass fiber and rubber particle-modified epoxy materials with PVDF and PEI interlayers using SENB experiments and modeling techniques. The results showed that interlayered finite element models can be used to assess the stiffness and crack shielding capabilities. PVDF and PEI interlayers were effective in deflecting and arresting cracks in non-toughened and toughened epoxy materials, with PEI showing better load resistance. Toughened epoxy designs showed enhanced toughness due to interlayering and plastic energy dissipation, but dual interlayering reduced fracture performance. Interface failure is the critical failure mode that can be mitigated by enhancing the thermoplastic-epoxy interface energy. Apart from the strength and stiffness, the fracture toughness of the interlayer material should also be considered. Macro voids introduced during the material application process significantly decreased crack reinitiation load and plastic-energy dissipation.

ACKNOWLEDGEMENTS

The authors wish to acknowledge the support and funding of this research by the Swiss National Science Foundation, Switzerland (https://www.snf.ch/en) under the project “Bonded composite primary structures in engineering applications (BONDS, Grant No. IZCOZ0_189905)”. The authors also acknowledge the experimental assistance provided by the technical team of the structural engineering experimental platform (GIS-ENAC at the Ecole Polytechnique Fédérale de Lausanne (EPFL), Switzerland). The authors also thank Gurit (UK) Ltd for providing the adhesive materials. This article/publication is based upon work from COST Action CA18120 (CERTBOND - https://certbond.eu/), supported by COST (European Cooperation in Science and Technology).

REFERENCES

[1] J.D. Pribe, T. Siegmund and J.J. Kruzic, The roles of yield strength mismatch, interface strength, and plastic strain gradients in fatigue crack growth across interfaces, *Engineering Fracture Mechanics*, 235, 2020, 107072. doi:10.1016/j.engfracmech.2020.107072.

[2] O. Kolednik, J. Predan, F.D. Fischer and P. Fratzl, Bioinspired design criteria for damage-resistant materials with periodically varying microstructure, *Advanced Functional Materials*, 21, 2011, 3634–3641. doi: 10.1002/adfm.201100443.

[3] O. Kolednik, R. Kasberger, M. Sistaninia, J. Predan and M. Kegl, Development of damage-tolerant and fracture-resistant materials by utilizing the material inhomogeneity effect, *Journal of Applied Mechanics*, Transactions ASME. 86, 2019. doi: 10.1115/1.4043829/726197.

[4] P. Fratzl, H.S. Gupta, F.D. Fischer and O. Kolednik, Hindered Crack Propagation in Materials with Periodically Varying Young's Modulus—Lessons from Biological Materials, *Advanced Materials*, 19, 2007, 2657–2661. doi: 10.1002/adma.200602394.

[5] A. Tiwari, J. Wiener, F. Arbeiter, G. Pinter and O. Kolednik, Application of the material inhomogeneity effect for the improvement of fracture toughness of a brittle polymer, *Engineering Fracture Mechanics*, 224, 2020, 106776. doi: 10.1016/j.engfracmech.2019.106776.

[6] M. Grossman, D. Pivovarov, F. Bouville, C. Dransfeld, K. Masania and A.R. Studart, Hierarchical Toughening of Nacre-Like Composites, *Advanced Functional Materials*, 29, 2019 1806800. doi: 10.1002/adfm.201806800.

[7] D.V. Srinivasan and A.P. Vassilopoulos, Fatigue performance of wind turbine rotor blade epoxy adhesives, *Polymer Testing*, 121, 2023 107975. doi: 10.1016/J.POLYMERTESTING.2023.107975.

[8] D.V. Srinivasan and A.P. Vassilopoulos, Manufacturing and toughening effects on the material properties of wind turbine blade adhesives, *Polymer Testing*, 116, 2022, 107770. doi: 10.1016/J.POLYMERTESTING.2022.107770.